Research Article

TRANSPARENT PROCESS SOURCE DATA OPEN ACCESS

Life Science Alliance

Engineered RNA biosensors enable ultrasensitive SARS-CoV-2 detection in a simple color and luminescence assay

Anirudh Chakravarthy[1,2,*], Anirudh Nandakumar[3,4,*], Geen George[1,*], Shyamsundar Ranganathan[5], Suchitta Umashankar[3], Nishan Shettigar[3], Dasaradhi Palakodeti[1], Akash Gulyani[6], Arati Ramesh[3]

The continued resurgence of the COVID-19 pandemic with multiple variants underlines the need for diagnostics that are adaptable to the virus. We have developed toehold RNA–based sensors across the SARS-CoV-2 genome for direct and ultrasensitive detection of the virus and its prominent variants. Here, isothermal amplification of a fragment of SARS-CoV-2 RNA coupled with activation of our biosensors leads to a conformational switch in the sensor. This leads to translation of a reporter protein, for example, LacZ or nano-lantern that is easily detected using color/luminescence. By optimizing RNA amplification and biosensor design, we have generated a highly sensitive diagnostic assay that is capable of detecting as low as 100 copies of viral RNA with development of bright color. This is easily visualized by the human eye and quantifiable using spectrophotometry. Finally, this PHAsed NASBA-Translation Optical Method (PHANTOM) using our engineered RNA biosensors efficiently detects viral RNA in patient samples. This work presents a powerful and universally accessible strategy for detecting COVID-19 and variants. This strategy is adaptable to further viral evolution and brings RNA bioengineering center-stage.

DOI 10.26508/lsa.202101213 | Received 2 August 2021 | Revised 11 September 2021 | Accepted 20 September 2021 | Published online 30 September 2021

Introduction

The COVID-19 pandemic has affected millions of people and caused severe disease, mortality, and disruption to human activity across the world. Current estimates suggest that at least 127.8 million (as of 31 March, 2021, WHO) people have been infected, and millions remain susceptible to this infection. The situation is compounded by the emergence of new variants of the virus, including potentially highly infectious strains. The COVID-19 disease is caused by a novel coronavirus SARS-CoV-2, belonging to the *Betacoronavirus* genus under the *Coronaviridae* family of viruses (1). Because of the large numbers of potential infections, the high infectivity of the virus and the wide diversity in the clinical presentation of the SARS-CoV-2 infections, there is an ongoing need for reliable and efficient diagnostic methods. This is especially felt because a substantial portion of human subjects infected with SARS-CoV-2 are asymptomatic or show very mild symptoms but may still remain infectious. Furthermore, amongst symptomatic COVID-19 patients, there is a wide variability in the nature and presentation of symptoms (2, 3). Therefore, the direct detection of SARS-CoV-2 infections remains important. Furthermore, detection strategies need to keep up with the evolving viral variants.

Currently, diagnostic testing of human subjects for SARS-CoV-2 infections broadly rely on either RNA amplification based methods or methods for detecting the presence of viral antigens (4, 5, 6, 7, 8). The current gold standard for testing remains the reverse transcriptase-quantitative-PCR (RT-qPCR) (9, 10) where amplification of one or more regions of viral RNA is typically detected with Taqman probes (11, 12, 13). Although the RT-PCR–based assay is considered more reliable for detection of virus, it involves significant processing steps and depends on the availability of sophisticated and expensive equipment, technical experts for instrument handling, and analysis of data. Another detection method is the reverse transcriptase coupled–loop mediated isothermal amplification (RT-LAMP). In typical RT-LAMP assays, amplification of DNA from viral RNA fragments is detected using dyes sensitive to pH, DNA, or pyrophosphates (14, 15, 16 *Preprint*). This method is relatively faster but may generate false positives because of non-specific amplification and primer interactions (17, 18). The CRISPR-Cas system has also emerged as an alternative platform for viral RNA detection. Here, CRISPR-Cas recognition of viral RNA is coupled with RNA amplification (19, 20, 21, 22, 23 *Preprint*) or used in an amplification-independent way via the use of more than one guide RNAs (24). These are currently restricted to a lateral flow assay format for colorimetric detection or use a fluorescence read-out, which may not lend itself to deployment in a variety of settings.

As a strategy for simple and specific SARS-CoV-2 detection that is compatible with a range of assay formats, we focused on direct detection of viral RNA fragments using an RNA biosensor approach.

[1]InStem–Institute for Stem Cell Science and Regenerative Medicine, Bangalore, India [2]SASTRA University, Tirumalaisamudram, Thanjavur, India [3]National Centre for Biological Sciences, GKVK Campus, Bangalore, India [4]Trans-Disciplinary Health Sciences and Technology, Bangalore, India [5]Red Hat, Inc., Westford, MA, USA [6]Department of Biochemistry, School of Life Sciences, University of Hyderabad, Hyderabad, India

Correspondence: arati@ncbs.res.in; akash.gulyani@uohyd.ac.in
*Anirudh Chakravarthy, Anirudh Nandakumar, and Geen George contributed equally to this work

RNA biosensors have been previously used for diverse sensing and diagnostics applications (25, 26). We searched for an RNA biosensor scaffold that was versatile, could be developed to be highly selective to SARS-CoV-2 RNA, could be used in a simple color read-out and where multiple steps of amplification built into the assay would result in high sensitivity/specificity. The previously reported toehold RNA scaffolds met these criteria and have been widely used for detecting other viruses (27, 28).

Toehold RNAs are synthetic switches that when placed in tandem, upstream of an mRNA, can control its translation (29, 30, 31, 32, 33, 34) (Fig 1A). In a typical configuration, a toehold switch consists of a central stem containing a ribosome binding site (RBS), a translation start site and a downstream reporter gene. A part of the central stem along with a 5′ overhang is designed to specifically base pair and bind with a Trigger RNA in *trans*. In the absence of the trigger, the central, conserved stem loop sequesters the region around the RBS and start codon, not allowing translation initiation. However, binding of the Trigger RNA to the biosensor disrupts the central stem, leading to a clear conformational switch in the sensor, exposing the RBS and start codon. This leads to translation of a reporter protein such as lacZ that can be easily detected using a chromogenic substrate.

In this study, using toehold switches as a starting point, we have engineered RNA biosensors that are highly selective for SARS-CoV-2 RNA. Isothermal amplification of SARS-CoV-2 RNA fragments, coupled with activation of our biosensors leads to production of lacZ protein. Subsequent cleavage of a chromogenic substrate results in a simple color assay for viral detection. In vitro characterization of these biosensors and testing of patient samples using our assay reveals a sensitivity up to 100 copies of viral RNA, making our biosensor a feasible module for detecting SARS-CoV-2 infection in patients. Notably, our biosensor detects a region of viral RNA that is conserved across all prominent variants (such as the α, β, γ and δ variants). We find that this assay is compatible with different modalities of detection wherein viral RNA is detected via luminescence, in a shorter period of time. By developing new biosensors, we offer PHANTOM (PHAsed NASBA-Translation Optical Method), an ultrasensitive, highly accurate COVID-19 detection platform that does not require any sophisticated equipment and is usable even in a low resource setting.

Results

Analysis of the SARS-CoV-2 genome and design of potential biosensors

Toehold sensors are designed to specifically recognize and respond to a region of viral RNA (called Trigger RNA). Each biosensor consists of a sensing region contiguous with a conserved stem-loop structure that contains a RBS and a translation start site followed by a reporter gene (Fig 1A). In the absence of viral RNA, the stem-loop sequesters the region around the RBS and the translation start site, thus keeping the biosensor "off." Binding of viral RNA to the sensing region causes a rearrangement of the biosensor, increasing accessibility of the otherwise inaccessible RBS. This leads to increased translation of the downstream reporter gene, leading to color production.

For a toehold-based biosensor to work, it requires extensive complementarity to its target viral RNA (Fig 1A). In addition to this, an ideal sensor would need to be sensitive in detection. To gain sensitivity, previous studies on toehold sensors coupled RNA amplification with sensing (27, 28, 29). To detect a wide range of SARS-CoV-2 RNA viral loads, we anticipated a need for RNA amplification (Fig 1B). Nucleic acid sequence–based amplification (NASBA) is an isothermal RNA amplification method, which relies on a pair of primers and the activity of three enzymes, Reverse transcriptase, RNaseH, and T7 RNA polymerase to gain up to 10^9-fold amplification (35, 36, 37, 38, 39, 40, 41, 42, 43).

To design suitable primers for NASBA (RNA amplification), we performed in silico analyses of the SARS-CoV-2 RNA genome, specifically the strain MT012098.1 from India (44) (Fig 1C). 20- to 24-nucleotide reverse (P1) and forward (P2) primers were designed to anneal throughout the viral genome. The criteria listed by Pardee et al (2016) (27) were adapted, wherein primers that end with "A," do not have four or more continuous repeats of any nucleotide, have a 40–60% GC content and a Tm greater than 41°C were selected. P1 and P2 primers that anneal within 120–170 nucleotides of each other were paired and primer pairs were scored using the software Primer3 (45) and NUPACK (46). Each primer pair thus results in a 120 to 170-nucleotide region referred to as Amplicon (Fig 1C).

Within the amplicons, using sliding windows of 36 nucleotides, we searched for contiguous single-stranded regions that would be accessible to the biosensor and would serve as the Trigger RNA (Fig 1C). The complementary sequence to each Trigger RNA was then incorporated into the toehold scaffold to generate SARS-CoV-2–specific biosensors. These potential biosensors were analyzed using NUPACK, and scored on the basis of the following parameters- (1) probability of formation of the lower stem (which is meant to enforce a stable "off state" of the sensor), (2) trigger single strandedness within the context of the amplicon (to increase accessibility of the trigger to bind the sensor), (3) single strandedness of the first 25 nucleotides of the sensor (meant to open the biosensor upon trigger binding) and finally the similarity to the desired consensus structure of the biosensor.

Based on these analyses we selected biosensors that (1) show high probability of forming the required sensor structure where, in the absence of viral RNA the "sensing region" and its complement are base-paired and (2) the sensing region and trigger are largely open to allow for base-pairing that allows opening of the switch. 19 potential biosensors with a diversity of scores for different parameters were taken further for in vitro studies (Tables S1 and S2 and Fig 2A and B). Overall, our computational pipeline yields a repertoire of biosensors capable of detecting different regions spread across the viral RNA genome.

Screening and identification of biosensors that detect SARS-CoV-2–derived RNAs

To test which of the designed sensors respond to their respective Trigger RNAs (synthetic RNAs identical to a portion of SARS-CoV-2 RNA), we used an in vitro transcription-translation (IVTT) coupled assay. In the absence of Trigger RNA the sensing region of the biosensor would base-pair with its complementary sequence, keeping the RBS and translation start codon inaccessible, hence keeping the

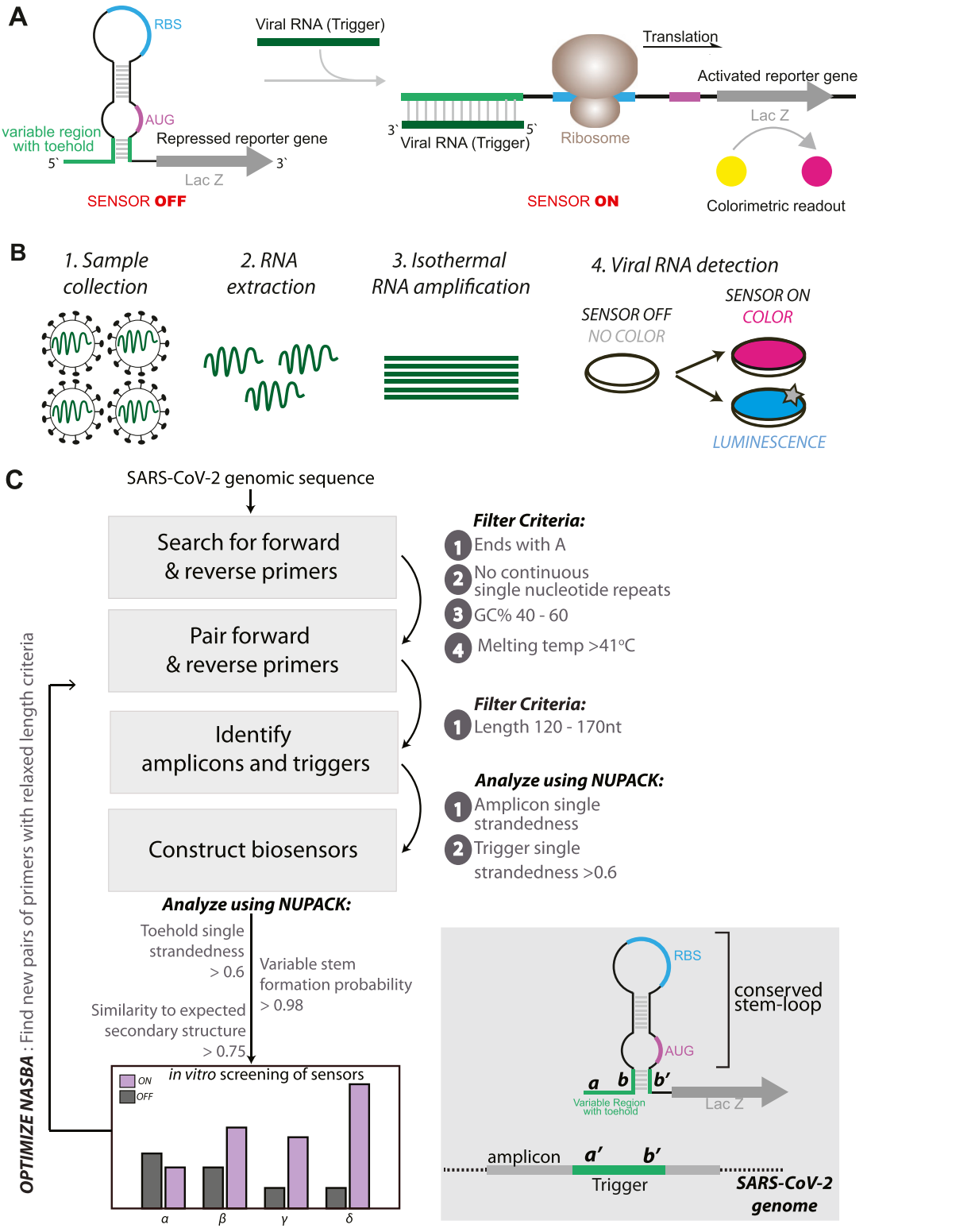

Figure 1. Concepts and design of SARS-CoV-2 RNA biosensors.
(A) Schematic of toehold switches. Toehold RNA switches consist of a central stem loop structure that harbors a ribosome binding site (RBS, blue) and a translation start site (AUG, pink) with a downstream reporter gene (such as *lacZ*, grey). A variable region with the toehold (green) is designed to specifically base-pair with a Trigger RNA (dark green). In the absence of Trigger RNA (left), the RBS and AUG are sequestered within the sensor structure and inaccessible to the ribosome. Presence of the Trigger RNA (right) induces intermolecular interactions between the toehold and the Trigger RNA, resulting in an alternate conformation wherein the RBS and AUG are accessible to the ribosome, enabling translation of the downstream LacZ enzyme. Production of LacZ is easily monitored with color, using a chromogenic substrate. The

sensor in its OFF state. Presence of the Trigger RNA would sequester the sensing region, thus exposing the RBS and start codon to enable translation of the downstream lacZ mRNA. This Trigger RNA-dependent production of lacZ protein is detected using colorimetry.

We tested 19 predicted sensors for their ability to produce color in the presence of Trigger RNA (Fig 2A). DNA corresponding to the biosensor was generated with a T7 promoter site at the 5′ end. This DNA when used as a template in the IVTT assay transcribes the RNA biosensor in situ. IVTT performed in the absence and presence of Trigger RNA were compared on the basis of Absorbance at 576 nm, which reports on the extent of cleavage of ChlorophenolRed-β-D-galactopyranoside (CPRG), a sensitive, red-shifted substrate of lacZ (47).

We find that all of the tested sensors showed absorbance at 576 nm in the presence of Trigger RNA. However, 12 of these sensors also showed detectable absorbance (>0.5 A_{576}) in the absence of Trigger RNA, suggesting leaky expression of *lacZ* and potentially unstable "off" state RNA conformations for this subset of sensors (Fig 2A). Notably, seven sensors show low absorbance (<0.5 A_{576}) in the absence of Trigger RNA and an increase in absorbance in the presence of trigger RNA (on/off A_{576} ratio > 14.0). Four of these sensors (1, 10, 12 and 17) with a high fold-change in absorbance (i.e., minimal *lacZ* expression in the "off" state and a substantial increase in *lacZ* expression in the presence of trigger RNA) were chosen for further analyses.

We next examined these four sensors for sensitivity of detection. Sensors 1, 10, 12, and 17 were used as template in IVTT assays in the presence of increasing amounts of Trigger RNA (Fig 2C–F). These sensors show sensitivity towards 10^{12} to 10^{13} copies of Trigger RNA. These experiments show that all four sensors respond to their respective Trigger RNAs, with a clear sensitivity threshold (Fig 2C–F).

Isothermal amplification of RNA to enable sensitive detection by biosensors

The inherent sensitivities observed for our sensors do not lie in a range that may be useful for unaided detection of SARS-CoV-2 RNA from infected patients' samples. For example, whereas viral loads are subject to much variation across populations and nature of infection (48), viral loads ranging from 10^8 to 10^3 copies/ml (at the limit of detection for RT-qPCR based testing) have been observed in naso-pharyngeal swabs of patients (49). Mean viral loads observed in nasopharyngeal swab samples and saliva samples are around 10^5 copies/ml approximately (50, 51). To use these sensors as diagnostic tools to detect SARS-CoV-2 infection, we coupled the IVTT assay with RNA amplification. This way the RNA to be sensed is amplified to amounts that are detectable by the biosensors. Nucleic acid sequence–based amplification (NASBA) is an isothermal RNA amplification method that can be coupled with toehold sensors (schematic in Fig 3A). Here, RNA (such as the viral genomic RNA) acts as template for reverse primer (P1) binding, which initiates reverse transcription at a particular position. cDNA first strand synthesis and removal of the template RNA strand by RNaseH enables binding of the forward primer (P2) which is designed to contain a T7 promoter region. This allows synthesis of the second strand of DNA. The resulting double-stranded DNA product is transcribed wherein each resulting RNA (RNA amplicon) once again serves as template for P1 binding and subsequent amplification.

To assess the sensitivity of our assay when coupled with NASBA amplification, we used a 127-nucleotide RNA fragment of the SARS-CoV-2 genome that encompassed the trigger for sensor 12 as a template. Increasing amounts of this RNA fragment were subjected to NASBA amplification followed by IVTT (Fig 3B). We find that when coupled with NASBA amplification, there is clearly detectable increase in absorbance even with 10^5 copies of the RNA fragment. In stark contrast, without NASBA amplification, a minimum of 10^{12} copies of the same RNA is required to elicit a color change. Coupling with NASBA amplification thus appears to increase the sensitivity of our assay with sensor 12 by nearly 10^7-fold, bringing these sensors into the realm of useful detection strategies for SARS-CoV-2 RNA in patient samples.

A key feature of NASBA that determines its efficiency is the selection of suitable primer pairs. We therefore further mined our list of NASBA primers in the region around the trigger for sensor 12. Here, we looked for primers that would generate amplicons sized 90–250 while encompassing the trigger for sensor 12. These additional primer pairs were first screened for their ability to amplify a template RNA at 10^8 copies (Fig S1A). Successful primer pairs were shortlisted and further screened for their ability to amplify 10^4 copies of template RNA (Fig S1B). The best primer pair was used in a NASBA reaction coupled with IVTT to evaluate the overall sensitivity of the assay (Fig 3C). For this test, we moved to using the widely accepted, commercially available SARS-CoV-2 Synthetic RNA (Twist Biosciences) (19, 52, 53) as template. Our results show that the best primer pair increases the efficiency of NASBA so that the effective sensitivity of our assay with sensor 12 is 100 copies of SARS-CoV-2 Synthetic RNA. A notable advantage of our assay is the facile color-based read-out that is amenable to easy detection and quantification. We find that the color produced in response to even 100 copies of RNA is easily detected with a basic cell-phone camera (Fig 3D). Put together, these data highlight that combining a suitable primer pair with our biosensor enables an ultrasensitive response to even small numbers of viral RNA copies that is easily visualized. Our initial experiments suggested that sensor 17 was inherently

concept is modular and allows the use of alternate reporter genes and modes of detection. **(B)** Schematic showing our assay development pipeline. RNA extracted from viral particles is amplified isothermally using (NASBA) nucleic acid sequence–based amplification and detected with specifically designed toehold-based biosensors in an in vitro transcription-translation assay. The NASBA coupled in vitro transcription-translation assay leads to production of color that can be easily visualized by eye or with cell phone cameras or luminescence that can be quantified by luminometry. Our assay development pipeline focused on identifying targetable regions of the SARS-CoV-2 genome, design of specific biosensors, optimized primers for efficient NASBA, and overall sensitivity and response of the assay. **(C)** Flowchart showing the bioinformatic pipeline for primer design, and selection of biosensors. First, we searched for primers that would amplify fragments of the SARS-CoV-2 genome, with criteria as highlighted in the figure. Amplicons resulting from primer pairs were analyzed for potential Trigger regions. Amplicon and Trigger single strandedness were estimated. These Trigger regions were used to construct the biosensors, which were then analyzed for toehold single strandedness, stem probability and fidelity to the expected biosensor secondary structure. Illustration (bottom right) shows the elements of the biosensor and Trigger RNA in detail.

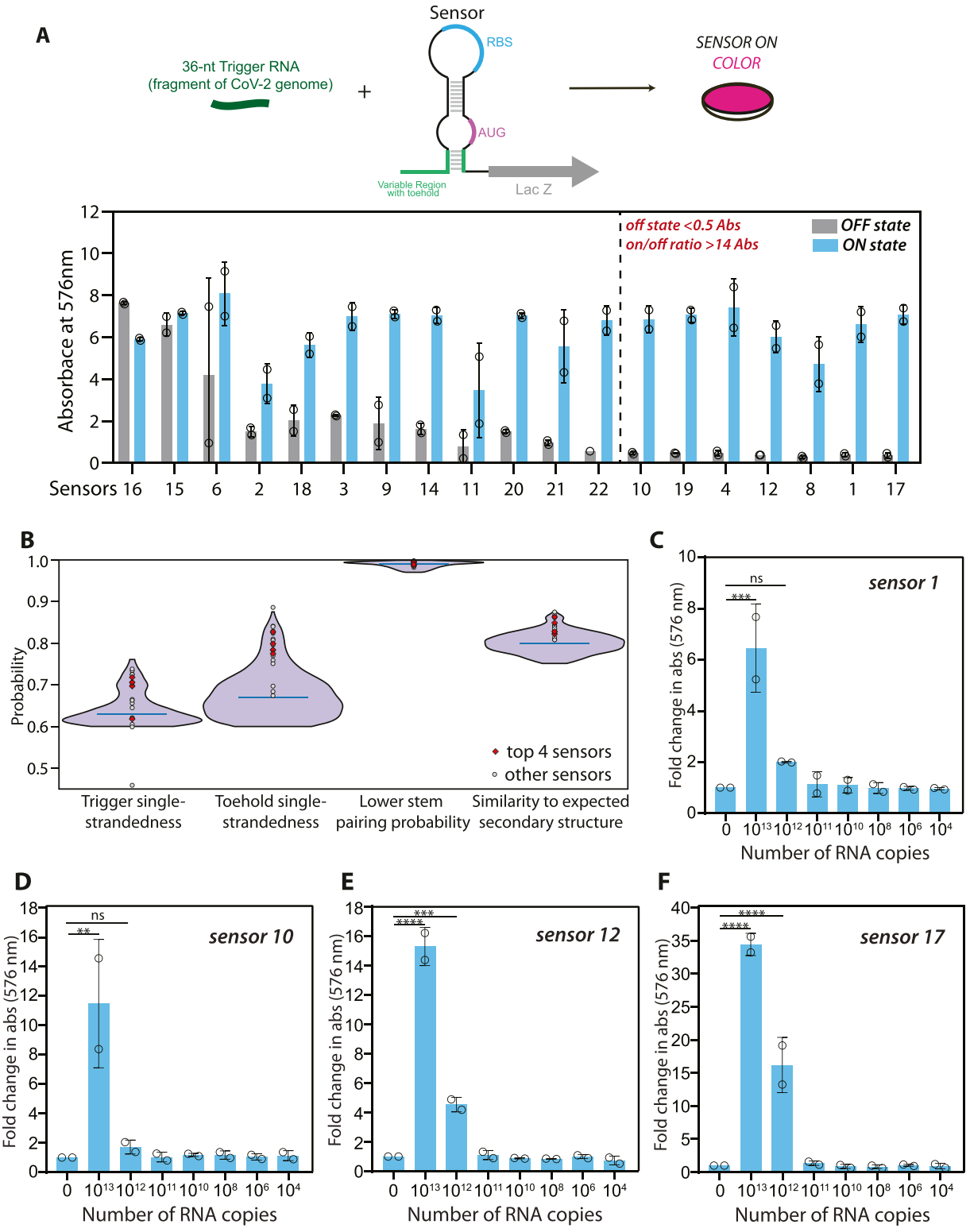

Figure 2. Screening and selection of SARS-CoV-2–responsive biosensors.
(A) In vitro transcription-translation assay performed on 19 shortlisted sensors was monitored using CPRG, a chromogenic substrate for lacZ. Absorbance (576 nm) is plotted for each sensor, in the presence (blue) or absence (grey, OFF state) of Trigger RNA. Dotted line separates seven sensors 1, 4, 8, 10, 12, 17, and 19 which show the maximum change with respect to the off state. This panel shows a preliminary screen (n = 2) that was carried out for 19 sensors. Screening was performed on potential sensors shortlisted based on the bioinformatics scores. **(B)** Results of the bioinformatic analysis are shown. Violin plot shows the probability distribution of different sensors with respect to four parameters-trigger single-strandedness, toehold single-strandedness, probability of formation of the lower stem, and similarity to the

more sensitive than sensor 12 (Fig 2E and F). However, when coupled with a step of NASBA amplification, the screen to identify pairs of NASBA primers gave us better hits for sensor 12, allowing detection down to 100 copies of RNA. Hence, we chose sensor 12 for further experiments.

We examined if sensor 12 is selective for the cognate region of the SARS-CoV-2 genome. To this end, we generated 19 different Target (Trigger) RNAs spread across the SARS-CoV-2 genome and tested them for their ability to turn on Sensor 12. We find that our sensor is highly selective for its cognate target RNA and does not show any detectable response to the other regions of SARS-CoV-2 (Fig S2A and B). We further examined specificity of our assay to SARS-CoV-2 versus other related human corona viruses. For this, we first examined the RNA sequence including and around the cognate target RNA for Sensor 12. We took equivalent regions from three strains belonging to the HCoV-HKU1 human coronavirus family (sequence alignment shown in Fig S3A) and generated these RNA sequences in vitro for IVTT. We find that these HKU1 human coronavirus RNAs are not able to turn on our sensor, whereas the cognate SARS-CoV-2 RNA is able to do so (Fig S3B).

Luminescence detection accelerates assay response to SARS-CoV-2 RNA

The biosensor design used here is modular and amenable to diverse read-outs, wherein the reporter gene can be switched from one to another (Fig 4A). The lacZ based readout used thus far allows for easy visualization of color in a sensitive manner. An important aspect of a diagnostic assay is the time taken to build a measurable response. To address this, we used the SARS-CoV-2 Synthetic RNA (Twist Biosciences) as input for NASBA and monitored the kinetics of the IVTT reaction (post-NASBA). We see a clear graded response to the copy number of RNA, with a faster build-up of color for higher initial RNA concentrations. 10^6 copies of RNA show discernible color (A_{576} > 1) even at ~60 min, whereas 100 copies of RNA are detectable at 100 min (Figs 4B and S4A–C). We tested the response of a luminescence based biosensor by replacing lacZ with the Nano-lantern protein, a fusion of Renilla Luciferase8 and the mTurquoise2 fluorescent protein (Figs 4C and S4D–F). We find the sensitivity of our assay remains conserved with detection of 100 copies of initial RNA template. Notably, the response is accelerated and even in 35 min we are able to detect substantial buildup of luminescence with 100 copies of RNA (Fig 4C and D). These results confirm that our SARS-CoV-2 biosensor is compatible with diverse read-outs, which can be used based on equipment availability and local needs.

Detecting SARS-CoV-2 RNA in patient samples

Having established assay sensitivity down to 100 RNA copies for sensor 12, we checked if this biosensor could detect SARS-CoV-2 RNA in patient samples (Figs 5A and S5A and B). To this end, we sampled RNAs extracted from nasopharyngeal swabs of 47 human subjects, whose samples had been tested with the standard RT-qPCR method (at the inStem-NCBS COVID-19 testing Center, Bangalore). Samples spanning a range of Ct values from the RT-qPCR test were tested with our assay. Samples with Ct values from 35 to 16 through a standard RT-qPCR assay (patients designated positive for COVID-19 infection) showed discernible buildup of color (absorbance at 576 nm) in our assay (Figs 5A and S5A and B). Importantly, the color produced in these samples is bright and easily detected by eye and is quantifiable through a cell-phone camera (Fig 5B). Absorbance changes observed in our assay correlate well with Ct values from RT-qPCR, and hence correlate with the amount of viral load in the patient samples. Three samples with Ct values 36–38 were indistinguishable from samples designated negative (Ct > 40) as well as the OFF state of the biosensor, indicating the possible limit of the assay in the absorbance mode. Importantly, the 27 samples with Ct > 40 (from subjects designated negative for COVID-19 infection) showed no significant absorbance in our assay and no discernible color either by eye or through a cell-phone camera photo. To assess the performance of our assay, we compared it with the RT-qPCR test as a benchmark, as is typically carried out for other COVID-19 diagnostics (19, 54 *Preprint*, 55). Analysis of these clinical samples detected through our assay showed 85% sensitivity and 100% specificity for our assay as compared with the RT-qPCR assay for COVID-19 detection (Fig 5C).

In the luminescence mode, we see a similar detection of positive patient samples ranging from Ct 16 up to ~Ct 35 and a clear discrimination from the negative samples (Figs 5D and E and S6A and B). In this range of Ct values, the signal is detectable at 30 min post-amplification (Fig 5D and E). For the range of Ct values 30–35, the signal is further enhanced between 30 and 50 min post-amplification (Figs 5E and S6C and D). Thus, our biosensor appears to be sensitive to the amount of SARS-CoV-2 RNA typically encountered in the population, and the readout is specific (no color/luminescence from negative samples).

A major cause of concern is the ability of SARS-CoV-2 to accumulate mutations in its genome. Bioinformatic examination of the trigger region recognized by sensor 12 and the regions recognized by the NASBA primers reveals strong conservation among all reported SARS-CoV-2 sequences, especially the prominent variants reported for SARS-CoV-2 (the α, β, γ variants). This implies that our

overall expected secondary structure of the biosensor. The violin plot was generated using the violin plot API in the python matplotlib package with default parameters except the width of violin (0.9), and number of points used to define the Gaussian kernel density (800). The blue line shown in the violin plot represents the median. Data from 759 sensors that met our filter criteria were included while generating the violin plot. 19 sensors were chosen for initial screening, based on their diversity of scores (grey circles). Four sensors (red diamonds) were further tested. **(C, D, E, F)** In vitro transcription–translation assays performed on four selected sensors (1, 10, 12, and 17) were monitored using CPRG, a red-shifted, chromogenic substrate for lacZ. Colorimetric response was monitored as a function of respective Trigger RNA concentration. Fold change in absorbance (576 nm) is plotted (bars) for each sensor, with varying amounts of Trigger RNA (0 to 10^{13} copies of RNA). Fold change (open circles) is calculated relative to OFF state of sensor (sensor alone, no RNA added) and obtained from n = 2 independent experiments. Error bars represent SD. Statistical significance (*P*-value < 0.0021 "**," <0.0002 "***," <0.0001 "****") was calculated using a one-way ANOVA with Bonferroni correction. These data reveal a clear threshold RNA concentration at which the sensors are able to respond to the Trigger RNA.
Source data are available for this figure.

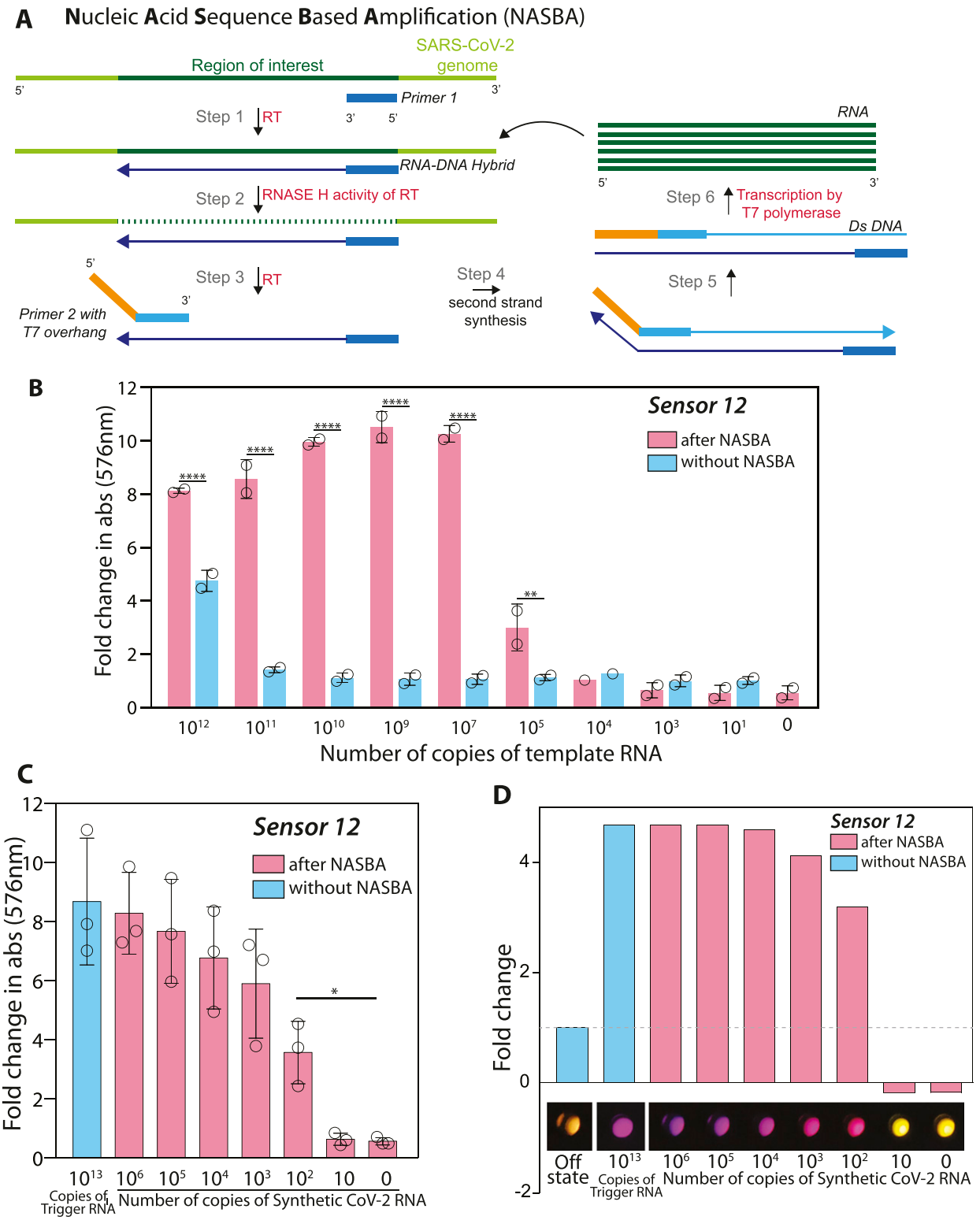

Figure 3. Isothermal RNA amplification (NASBA) allows for sensitive detection of SARS-CoV-2 RNA.
(A) Schematic for NASBA showing the various steps involved. RNA template is reverse transcribed by Primer P1 to form the first strand of cDNA. RNaseH activity degrades the RNA in the DNA:RNA hybrid. The resulting single stranded cDNA is recognized by primer P2 containing a T7 promoter sequence. After second-strand DNA synthesis, the resultant double stranded DNA acts as a template for T7-RNA polymerase based transcription resulting in several RNA molecules. Each newly synthesized RNA molecule in turn acts as a template for the next round of amplification, leading to iterative amplification. **(B)** In vitro transcription–translation assay performed with sensor 12, with and without NASBA amplification is shown. A synthetic RNA fragment of SARS-CoV-2 containing the trigger for sensor 12 was tested for its ability to activate the sensor on

detection strategy would work for these key variants. Of these variants, the δ variant (B.1.617.2) is not only highly contagious but has become the dominant variant in several populations (56, 57, 58). Given its importance, we tested to see if our assay can detect the δ variant in patient samples. For this, we obtained RNA from the nasopharyngeal swabs of patients from the NCBS-inStem COVID-19 testing Center. RNA was isolated in the BSL-3 facility at the testing center and sequenced and confirmed to be the δ variant B.1.617.2 (sequences deposited in GISAID). RNA extracted from these patient samples were tested against Sensor 12 using NASBA followed by IVTT. We find that our assay can efficiently detect the δ variant SARS-CoV-2 RNA from patient samples with a buildup of color, whereas no color was observed from control samples (Figs 5F and S7A and B). The ability to detect the δ variant of SARS-CoV-2 is an important feature of our sensor because this variant is now of global concern and extensively found in the population (56, 57, 58). Based on these collective data, we propose PHANTOM (PHAsed NASBA-Translation Optical Method) as a feasible module for unambiguous COVID-19 detection that is universally accessible in a variety of settings.

Discussion

In this report, using computational methods, we have designed toehold RNA–based biosensors that are tuned to sense different fragments of the SARS-CoV-2 RNA, spread across the genome. Extensive in vitro screening and characterization led us to identify biosensors that turn on translation of the reporter lacZ, in response to SARS-CoV-2 RNA fragments. Taking one of these biosensors forward, we coupled isothermal NASBA based RNA amplification to the IVTT assay to achieve sensitivities in the range of 100 copies of viral RNA. Alternate luminescence based detection enabled a faster time response post-amplification, highlighting the modularity of our system. When applied to patient samples, our assay provides a clear response that discriminates viral-positive from negative samples. Collectively, we present here a diagnostic platform with a read-out that is quantifiable and correlates excellently with the gold standard RT-qPCR assays. Furthermore, this assay can be deployed in a low resource setting as the read-out is easily visualized by eye as well as through a simple cell phone camera, and the assay itself does not require any expensive equipment.

A key advance of this work is to exploit the toehold concept for SARS-CoV-2 detection. The toehold switch concept itself is an elegant strategy for RNA detection that has been used successfully for viral infections and other pathologies (27, 28). A hallmark of this concept is an RNA-based switch that is designed for *specific* and *direct* detection of any RNA sequence. A key challenge in this toehold design is to ensure that the sensor is truly "off" in the absence of target RNA and turns on *only* in response to the target. We found that both the computational analyses and in vitro screening were crucial to overcome this challenge. We initially chose sensors with diverse scores across bioinformatic parameters. Combining this with targeted in vitro screening, we were able to identify the sensors that show a suitable ON to OFF state response.

The toehold switch concept is highly modular, allowing different reporters and hence diverse read-outs for detection (27, 28, 29, 30, 31, 32). We exploited this to develop two independent modes of detection, that is, color (using lacZ) versus luminescence (using nano-lantern). The production of bright color even at 100 copies of viral RNA allows for very easy visualization by eye, enabling a yes-no answer for the presence of viral RNA. To remove the subjective bias inherent in eye-based detection, we also show that the color produced in response to viral RNA can be recorded and validated through a basic cell phone camera. This feature of the PHANTOM assay would be extremely valuable in a low-resource setting because neither conducting the assay nor interpretation of its results require specialized equipment or training. This is aided by the fact that this assay is compatible with most formats and can be conducted in tubes, paper strips, or high-throughput multi-well plates. In a laboratory setting, both the luminescence as well as colorimetric read-outs can be measured quantitatively using a luminometer or spectrophotometer. Comparing the two modes of detection, we observe a significant decrease in response time wherein luminescence buildup is seen even in 30 min post-amplification. Here, it is possible that different extent/kinetics of translation of different reporters as well as their differences in their enzymatic activities play a role in determining the assay time.

Another significant step of optimization in our assay is during RNA amplification using NASBA. Previous reports have also highlighted the importance of primer design and optimization to achieve efficient NASBA (28, 52, 59). We observed that primers with fairly similar basic criteria showed significantly different NASBA efficiencies. Therefore, after an initial round of screening for sensors, and zeroing in on an efficient sensor, we again screened for the most efficient NASBA primers for the selected sensor. This was crucial in achieving the overall sensitivity of the assay. We could detect 100 copies of viral RNA and overall sensitivity of 8 aM viral RNA. Our results reveal the importance of empirical screening with a diverse set of primers for efficient NASBA.

With a robust and sensitive assay in hand, we asked if the time taken for this assay could be optimized further. One of the key steps

its own or post-NASBA amplification. Open circles represent the fold change values. Statistical significance (*P*-value < 0.0021 is shown as "**" and *P*-value < 0.0001 shown as "****") was calculated using a multiple unpaired t-test with a Sidak–Bonferroni correction. Fold change in absorbance (576 nm) is plotted (bars) against varying amounts of initial RNA (0 to 10^{13} copies of RNA), with (pink) and without (blue) NASBA. "0 RNA copies" denote no template control (primer + NASBA reaction mix, no RNA added). Fold change is calculated relative to OFF state (sensor alone). **(C)** NASBA coupled with in vitro transcription–translation assay performed using a commercially available synthetic SARS-CoV-2 viral RNA control (Twist Biosciences) as template. Fold change in absorbance (576 nm) is plotted (bars) against increasing amounts of viral RNA (10 to 10^6 copies of RNA). Data shown are from three independent experiments (n = 3), and error bars represent SD. Statistical significance (*P*-value < 0.0332 "*") was calculated using one-way ANOVA with Bonferroni correction. Trigger RNA at 10^{13} copies (blue) is used as a positive control. Results show a sensitivity of the assay down to 100 copies of viral RNA. **(D)** Samples from panel (C) were imaged using a cell phone camera. Representative image shows bright and discernible color even when starting with 100 copies of viral RNA as input. Color from individual wells was quantified and plotted as fold change relative to the off state.
Source data are available for this figure.

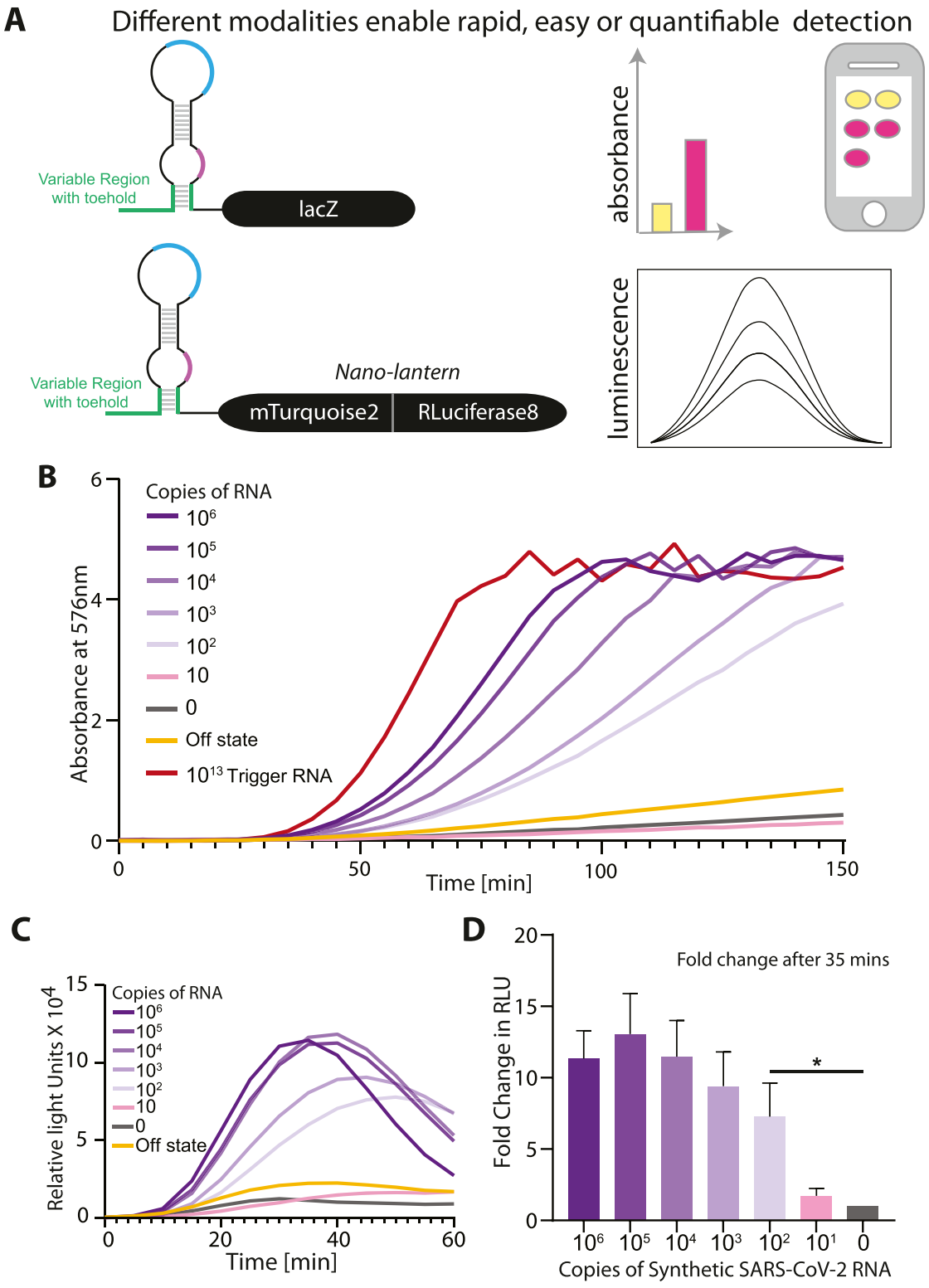

Figure 4. Luminescence read-out speeds up detection of SARS-CoV-2 RNA.
(A) Illustration shows the construction of biosensors with alternate modalities of viral RNA detection. Biosensors may comprise a color-producing enzyme such as lacZ or a luminescence producing system coupled to the RNA-binding module. For luminescence-based detection, the nano-lantern system (fusion of Renilla luciferase8 with mTurquoise2 fluorescent protein) was used. **(B, C)** NASBA coupled with in vitro transcription–translation (IVTT) assay performed using a commercially available synthetic SARS-CoV-2 viral RNA control (Twist Biosciences) as template. Sensor 12 fused to lacZ was used for IVTT. One representative time kinetics data from three independent experiments (n = 3) is shown. Individual plots of all three trials are shown in supplementary data, as Fig S4A–C. Panel (B) shows absorbance (576 nm) over time for varying

here is the NASBA amplification hence we tested to see if the time taken for NASBA could be decreased. We found that even at the limit of detection (i.e., 100 copies of viral RNA), we were able to complete the NASBA amplification step in ~60 min (Fig S8A–E). This, along with the faster luminescence detection effectively reduces the assay time to ~90 min or better.

Finally, our results with the human patients show that our assay can clearly distinguish viral-positive from negative samples. Indeed there is strong correlation between the assay response and Ct values obtained from the RT-qPCR test. The overall sensitivity in the attomolar range ensures detection of infection in most COVID-19–positive patients in a population. The GISAID database reports ~2,418,000 high quality sequenced genomes (as of 08 August, 2021) from different clades of the SARS-CoV-2 virus. The viral RNA fragment that turns on our sensor is located in the ORF1ab (Nsp13) region of the genome. This region is completely conserved in greater than 98.32% of deposited genomes of SARS-CoV-2. This indicates that our sensors would be capable of detecting nearly all of the currently sequenced strains of SARS-CoV-2. Most significantly, this region is invariant among 99.28% δ variant (B.1.617.2), 98.45% α (B.1.1.7) variant, and 99.62% and 99.41% in the γ (P.1) and the β (B.1.351) variants of SARS-CoV-2 respectively. Our data clearly show that the PHANTOM assay reliably detects the presence of the δ variant in patient samples. A feature of toehold-based biosensors is the multiple check-points for specificity in detection. One level of specificity comes from primers that amplify only a given region of the viral RNA and second comes from sequence-specific interactions between the viral RNA fragment and the biosensor. This is exemplified by our results wherein we observe very low false-positive rates. Detectable color is produced in positive patients (20 positive) but no color in negative patients (27 negative patients). Finally, our assay works well with the standard mode of nasopharyngeal sample collection. Combining this method of detection with other modes of sample collection such as saliva would be a significant advance going forward.

In conclusion, our engineered biosensors along with the PHANTOM platform provide a powerful strategy for COVID-19 detection. This can not only mitigate uncertainties in global supply chains and counter a shortage of reagents but also serve different local conditions and contexts that may benefit from diverse testing strategies.

Materials and Methods

Bioinformatic analysis and sensor design

To establish a pipeline for designing SARS-CoV-2–specific toehold sensors, we started by searching for primers that would anneal to the SARS-CoV-2 genomic RNA. An Indian strain of SARS-CoV-2 (accession code MT012098.1) was downloaded from National Center for Biotechnology Information (NCBI) and used for analysis.

Step 1: searching for primers

Using a custom program we divided the genomic sequence (and its reverse complement) into all possible fragments of 20–24 nucleotides. Fragments which end with an Adenosine, do not have a continuous stretch of four or more of the same nucleotide, show a GC content between 40 and 60%, and have a melting temperature above 41°C were shortlisted and considered as primers. Fragments arising from the sense strand were considered as forward primers (P2 primer) and were prefixed with a T7 promoter sequence (AATTCTAATACGACTCACTATAGGGAGAAGG). Fragments from the reverse complement were considered as reverse primers (P1 primer). All primers were scored using Primer3 (v. 2.5.0) (45) and NUPACK (v. 3.2.2) (46). Reaction conditions were defined as 41°C and buffer containing 50 mM sodium and 12 mM magnesium and primers were then scored based on the following parameters:

(1) First 6-nt GC count (including hybridized region for forward primers)
(2) Last 6-nt AT count
(3) Total % GC (including hybridized region for forward primers)
(4) Single strandedness
(5) Concentration of primer remaining in monomeric form
(6) Single strandedness of the last six nucleotides
(7) Contiguity length

Step 2: identifying targetable regions (Trigger RNAs) within the SARS-CoV-2 genome

Forward and reverse primers that are separated by 120–170 nucleotides (inclusive of primer length) are paired. The region amplified by each primer pair is considered as an amplicon. Single-strandedness of all resulting amplicons was estimated using the *complexdefect* function in the NUPACK package (46). For this amplicon analysis, we included the standard nine nucleotides (GGGAGAAGG) appended to each sequence at the 5′ end. Separately, for sensor 12 NASBA primer screening experiments (Fig S1), forward and reverse primers separated by 90–250 nucleotides (inclusive of primer length) were paired.

Each amplicon from the previous step was split into continuous windows of 36 nucleotides each. Each 36-nt sequence is considered a Trigger RNA. Using the *pairs* function in NUPACK, we calculated the pair probabilities for the whole amplicon. Using a custom code, we then extracted probabilities related to the Trigger regions. This Trigger single-strandedness (in the context of the whole amplicon) was considered for our analysis.

amounts of viral RNA (0–10^6 copies of RNA). Panel (C) shows relative luminescence intensity over time for varying amounts of viral RNA (0–10^6 copies of RNA). Trigger RNA at 10^{13} copies (red) is used as a positive control. For luminescence readout, sensor 12 was fused to the Nano-lantern reporter. One representative data from three independent experiments (n = 3) is shown. Individual plots of all three trials are shown in supplementary data, as Fig S4D–F. **(D)** Fold change (bars) in luminescence intensity for varying amounts of viral RNA (0–10^6 copies of RNA) after 35 min of the IVTT reaction post-NASBA. Fold change is calculated with respect to the "0" RNA NASBA reaction. Data shown are from three independent experiments. Error bars represent SD. Statistical significance (*P*-value < 0.0332 shown as "*") was calculated using a one-way ANOVA with Bonferroni correction.
Source data are available for this figure.

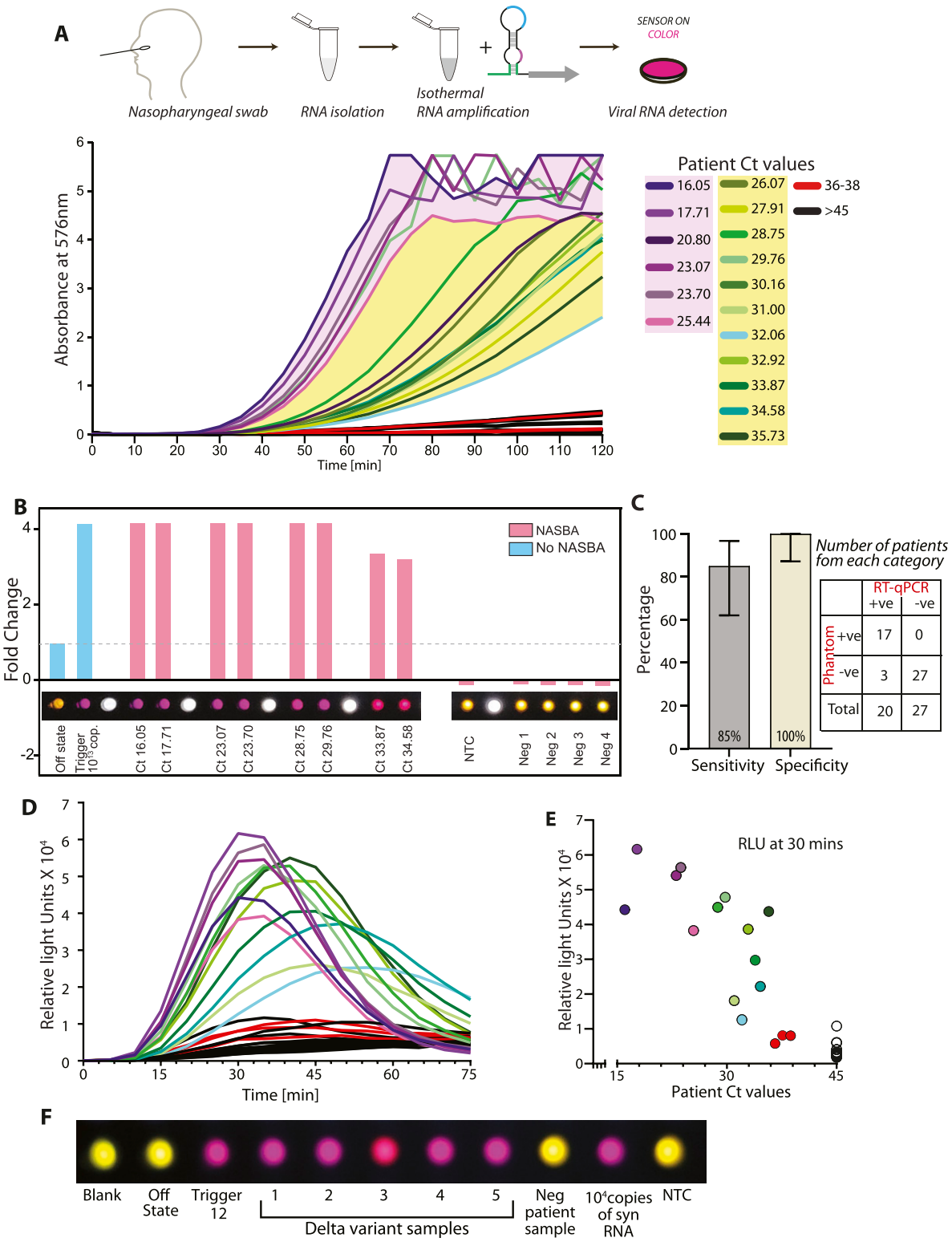

Figure 5. Sensitive and specific detection of SARS-CoV-2 RNA in human patient samples.
(A) NASBA coupled with in vitro transcription–translation (IVTT) assay performed on RNA extracted from nasopharyngeal swab samples. Samples had already been tested for the presence of SARS-CoV-2 RNA using standard real-time RT-PCR test and designated negative or positive (with accompanying Ct values shown here). Sensor 12 fused to lacZ was used for IVTT. Shown are absorbance (576 nm) values over time. Samples are color coded based on their designation and Ct values; Ct values 16–25.4 (purple), Ct values 26–35.7 (green), Ct values 36–38 (red), and negative patients with Ct values > 45 (black). Caption indicates Ct values corresponding to individual curves.
(B) Photo from a basic cell phone camera showing color readouts of IVTT assay from patient samples. Assay (as described in (A)) performed in plate format. Bar graph

Step 3: construction and analysis of biosensors

To construct the biosensors, the reverse complement of each Trigger sequence was appended to the 5′ end of the conserved stem-loop in the toehold design. The sequence of the conserved stem-loop was taken from Series B toehold sensors as described in Pardee et al (2016) (21) Thus, each complete biosensor (full sequences are given in Table S1) consists of 5′- reverse complement of trigger + conserved stem-loop + first 11-nt of trigger + (N1) + linker + reporter gene (lacZ/nano-lantern), where (N) is any nucleotide. To aid in efficient transcription, we ensured that for each sensor, the T7 promoter sequence was followed by 3Gs. Only sensors that do not possess a stop codon were considered further.

Using NUPACK, the sensors were analyzed for single strandedness of the toehold region (initial 25 nts + G's added) and the probability of formation of the lower (variable) stem (b–b* in Fig 1C). In addition, the region from the 5′ end to (inclusive of) the linker was separately analyzed for its similarity to the expected secondary structure (as described in Pardee et al [2016] (27)).

Step 4: choice of sensors for in vitro screening

Four parameters were considered while choosing sensors for in vitro screening. Trigger single-strandedness (>0.6), toehold single-strandedness (>0.6), probability of formation of the variable stem (>0.98), and the similarity to expected secondary structure (>0.75) were used as minimum criteria. From the list of sensors that passed these criteria, 25 sensors were chosen. Their trigger sequences were checked for potential similarity to the human genome (Accession code: 000001405.38) and transcriptome (Refseq, 16 May, 2020) using the megablast module of NCBI-BLAST, with default parameters (e-value threshold: 0.05, gap costs: creation −5 extension −2, match/mismatch score: +2/−3). Only the triggers that did not have any hits were chosen for in vitro analysis (sensor parameters in Table S2). 19 sensors meeting these criteria were picked for screening.

In vitro preparation of toehold biosensors

The complete DNA template for an RNA biosensor consists of the T7 promoter, sensor sequence with RBS and start codon, linker and the lacZ (or Nano-lantern) reporter gene. To construct this, we first cloned the linker (this is common to all sensors) in frame with the *lacZ* or nano-lantern gene in a standard *Escherichia coli* plasmid. Then, we purchased DNA oligos (listed in Table S3) containing the T7 promoter, sensor, RBS, the start codon, and the linker. A PCR was carried out to stitch this DNA oligo (T7 promoter to linker) with the linker-lacZ DNA, using relevant primers (Table S3). This results in a linear DNA template that was purified (Promega, Cat. no. A9282) and subsequently used as input to the IVTT assays.

In vitro transcription of Trigger RNAs and template RNAs

The RNA templates for NASBA reactions and Trigger RNAs for cell free IVTT reactions were synthesized by in vitro transcription reactions. This was done in a 40-μl in vitro transcription reaction system. Each reaction contained 2.5 μg of the relevant DNA template, 4 μl of 10X T7 polymerase reaction buffer (Toyobo, Cat. no. TRL-201), 5.5 μl of 50 mM $MgCl_2$, 4 μl of 25 mM rNTPs (NEB, Cat. no. N0450S), 2 μl (100 units) of T7 RNA polymerase enzyme (Toyobo, Cat. no. TRL-201), 2 μl (0.2 units) Yeast Inorganic Pyrophosphatase (NEB, Cat. no. M2403S), 0.5 μl (20 units) RNaseOUT (Invitrogen, Cat. no. 10777019), and the remainder of the reaction volume was made up to 40 μl with nuclease free water and incubated at 37°C for 2 h. After this, the samples were treated with 2 μl (4 units) of DNAse I enzyme (NEB, Cat. no. M0303S) at 37°C for 1 h and purified using the ZymoResearch RNA Clean and Concentrator RNA purification kit (Cat. no. R1015). The final RNA sample was eluted in nuclease free water for further use.

IVTT assay

Cell-free IVTT reactions (NEB PURExpress, Cat. no. E6800L) were prepared using the manufacturer's protocol. In a total reaction volume of 10 μl, 4 μl of solution A was added along with 3 μl of solution B, 0.25 μl (10 Units) of RNase Inhibitor (Thermo Fisher Scientific, Cat. no. 10777019), and 125 ng linear DNA template. Reactions were initiated with Trigger RNA or NASBA product wherever applicable and incubated at 37°C for 2 h. For IVTT reactions with Trigger RNA (Fig 2A), 1 μl of each 9 μM Trigger RNA stock was added to 10 μl cell-free reaction with respective sensors. For Trigger RNA dilutions (Fig 2C–F), a stock of Trigger RNA was prepared and serially diluted to obtain concentrations from 9 μM to 9 fM. These Trigger RNA concentrations were added to approximately obtain copies of 10^{13}–10^{4} in each reaction tube. For IVTT reactions initiated with NASBA products, 2.5 μl of the NASBA reaction was used as input.

For reactions with ChlorophenolRed-β-D-galactopyranoside-CPRG (Sigma-Aldrich, Cat. no. 59767), 0.75 μl of 12 mg/ml substrate was added from the start of the IVTT reaction and incubated at 37°C for 2 h. Samples were quenched with 2 μl of 2 M Na_2CO_3 absorbance recorded at 576 nm. Absorbance (576 nm) was recorded for the samples (at a dilution of 1:10), using a cuvette of path length 1 mm, on a Spectrophotometer (Eppendorf Biospectrometer). Fold

shows quantitation of individual wells showing color readouts from selected patient samples. A cell phone camera image can be used to distinguish COVID-19 positive from negative samples. **(C)** 20 COVID-19 positive and 27 negative samples as determined by RT-qPCR, were tested using our PHANTOM assay (contingency table). Sensitivity is calculated as the ratio of number of positives identified by our assay to the total number of RT-qPCR–positive samples tested. Specificity is calculated as the ratio of number of negatives identified by our assay to the total number of RT-qPCR–negative samples tested. Error bars represent 95% confidence interval calculated using the Exact Clopper Pearson method. **(D)** Luminescence read-out for patient samples. Sensor 12 fused Nano-lantern is used for IVTT assay. Shown are luminescence intensities for patient samples over time. Color coding of samples same as above. **(E)** Luminescence intensity at 30 min of the IVTT assay (post-NASBA amplification) versus Ct-value for patient samples. Ct values were determined through the standard real-time RT-PCR test. Assay read-out clearly discriminates samples positive for viral RNA from negative samples. **(F)** Photo from a cell phone camera showing color readouts of IVTT assay from δ variant (B.1.617.2) patient samples. Time course measurements are shown in Fig S7.
Source data are available for this figure.

change in absorbance was calculated relative to the sensor "OFF" state.

Alternately, we performed IVTT reactions in 384-well plates (Corning, Cat. no. 3544). Here, total IVTT reaction volume was proportionately reduced to 5 μl. Reactions were set up as described above and the plates were placed in a Varioskan Lux instrument (Thermo Fisher Scientific) set at 37°C. Absorbance was monitored at 576 nm, at 5 min intervals, for 150 min. The linear measurement range of the Varioskan Lux multiplate reader is 0–3 absorbance for a 384 well plate. The number of replicates for each experiment is indicated in the individual figure legends. Information on statistical tests carried out and statistical measures plotted are also indicated in the individual figure legends. All absorbance based plate reader experiments were first baseline corrected using a blank sample and each sample was normalized such that the lowest absorbance measurement was set to 0. All data were plotted using GraphPad Prism 8 and figures were made using Adobe Illustrator.

Mobile phone image acquisition and analysis

Post IVTT reaction, the Corning 384 well clear bottom microplate was placed upside down on a white LED light source. An RGB image was acquired using a smart phone camera (Xiaomi PocoF1, Redmi Note 9 Pro Max). Image was further processed and analyzed using Fiji/image J 1.52p (60). First, the RGB image was cropped into the required dimension. Second, the cropped RGB image was split into three independent 8-bit greyscale images (Red, Green, Blue components of the original image). Third, a uniform circular region of interest was drawn within the area of each well (green channel grayscale image), to determine the signal by averaging the pixel values. Blank well value was subtracted from all other well values. Finally, the fold change was quantified by using the average signal from sensor off state well.

Luminescence assays

For luminescence assays with Coelenterazine H (C3230-50UG; Sigma-Aldrich), 0.25 μl of 400 μM substrate was added from the start of the IVTT reaction. IVTT reactions were set up in 384-well plates as described above and monitored using the Varioskan Lux instrument (Thermo Fisher Scientific) set at 37°C. Intensity was measured in the "normal" luminescence mode without wavelength selection.

Isothermal RNA amplification (NASBA)

For NASBA reactions, a relevant RNA template from SARS-CoV-2 genome was made using in vitro transcription as described above. In a reaction volume of 17.7 μl, RNA template (ranging from 10 to 10^{13} copies) was incubated with 4 μl of 5X AMV RT Buffer (Roche, Cat. no. 10109118001), 1.6 μl of 50 mM $MgCl_2$, 2 μl of 25 mM rNTPs (NEB, Cat. no. N0450S), 2 μl of 10 mM dNTPs (NEB, Cat. no. N0447S), 0.18 μl of 1 M DTT (VWR, Cat. no. 3483-12-3), 3 μl of 100% DMSO (Sigma-Aldrich, Cat. no. D8418-50 Ml), 0.2 μl of 10 mg/ml BSA (Roche, Cat. no. 10735078001), and 0.5 μl each of 10 μM forward and reverse primers. The assembled reaction mix was initially incubated at 65°C for 5 min, followed by 50°C for 5 min, post which an enzyme mix containing 1 μl (50 Units) T7 RNA Polymerase (Toyobo, Cat. no. TRL-201), 1 μl (20 Units) AMV-RT (Roche, Cat. no. 10109118001) 0.1 μl (0.2 Units) RNaseH (Roche, Cat. no. 10786357001), and 0.2 μl (12.5 Units) of RNaseOUT (Invitrogen, Cat. no. 10777019) was added and the reaction was incubated at 42°C for 2 h. Post-NASBA, the samples were either stored at −80°C or taken further for IVTT assays.

For the initial NASBA experiments (Fig 3B), an RNA template of 127 nucleotides (corresponding to coordinates 17,673–17,799 of MT012098.1 accession code) was used at different starting copy numbers (10 to 10^{12}). A sequence of GGGAGAAGG was appended to the 5′ to increase transcription efficiency. For the NASBA primer screening experiments (in Fig S1), an RNA template of 3.1 kb (corresponding to coordinates 17,131–20,234 of MT012098.1 accession code) was used initially at 10^8 and subsequently at 10^4 copies. For testing the sensitivity of the best NASBA primer pair, a commercially available synthetic SARS-CoV-2 RNA (Twist Bioscience, Cat. no. 102024) was used. Design and rationale behind the choice of primers is described in the Bioinformatics section above. For patient samples that were tested (in Figs 5 and S5S–SS5–S7), 1 μl of RNA isolated from 150 μl of viral transport medium that contained isolates from nasopharyngeal swabs was used as template for NASBA. For the time course analysis of NASBA (Fig S8), reactions were set up as described above and terminated at 20, 40, 60, and 120 min, respectively.

A total of 28 primer sets were selected for sensor 12. Of these, 14 primer sets contained a forward primer (P2) with a minimal T7 promoter (TAATACGACTCACTATAGG), and are referred to as S01–S14 primer sets. The remaining 14 primer sets contained a longer T7 promoter with a purine stretch (AATTCTAATACGACTCACTATAGGGAGAAGG) as used in Deiman et al (2002) (61), and are referred to as L01 to L14 primer sets. The primer screen was carried out in two phases. The first phase involved the screening of all primer sets with 10^8 copies of RNA as starting material. This was done to shortlist all primer sets that were capable of amplifying the target RNA to enable their detection using our IVTT assay. From these experiments, we shortlisted the primer sets that showed the fastest development of color in our IVTT assays. A total of 11 primer pairs were shortlisted for the second phase of our screen. These primers were tested with only 10^4 copies of template RNA to identify primer sets that could better the sensitivity of our previously used primers. The primer set (primer pair: S01) that showed the fastest development of color and the highest signal to noise ratio was finally selected. NASBA Primer pairs for sensor 12 are listed in Table S4.

Data Availability

The datasets generated during and/or analyzed during the current study are available from the corresponding authors upon reasonable request. Custom software is deposited at Github (https://github.com/ShyamsundarR/silicasense) and available upon reasonable request.

Supplementary Information

Supplementary Information is available at https://doi.org/10.26508/lsa.202101213.

Acknowledgements

We are grateful to Professor Satyajit Mayor for unstinting support for this project and very insightful discussions. We also thank Prof. Mayor for help with continued funding for this project. For patient samples, we especially thank the inStem-NCBS testing facility and the Department of Biotechnology, Govt. of India for support of the inStem/NCBS COVID-19 Bioresource (BT/PR40403/COT/142/8/2020). We thank Prof. Apurva Sarin and Colin Jamora for support. We are grateful to the Azim Premji Philanthropic initiative, Punjab National Bank Housing, and IQVIA for funding. We acknowledge support from the Department of Atomic Energy, Government of India, and the National Centre for Biological Sciences-Tata Institute of Fundamental Research (TIFR), under project no. 12-R&D-TFR-5.04-0800. Research in the A Ramesh lab is also supported by the Human Frontier Science Program research grant RGY0077/2019 and DBT/Wellcome Trust-India Alliance (IA/I/14/2/501521). A Gulyani thanks University of Hyderabad, the School of Life Sciences and Department of Biochemistry (UoH), for support. We are grateful to Professor Dayananda Siddavattam for support and discussions. A Gulyani also thanks Professor Krishnaveni Mishra for support. Research in AG lab is also supported by Scientific and Engineering Research Board (SERB), DST, Govt. of India (EMR/2017/005093). All clinical patient samples from nasopharyngeal swabs, which underwent real time RT-PCR testing according the ICMR guidelines, were provided by the inStem-NCBS COVID-19 testing center. Approvals by the Institutional Human Ethics Committee (NCBS/IEC-17/002; inStem/IEC-17/001), the Institutional Biosafety Committee (TFR:NCBS:31-IBSC_UR; inStem/G-141(3)-15/CJ), and the Review Committee on Genetic Manipulation-RCGM (BT/BS/17/371/2010-PID) were obtained for conducting the RT-PCR protocols on clinical patient samples, for the presence of SARS-CoV-2 RNA. Separate RCGM approval was obtained for testing the toehold sensors (Document No BT/IBKP/035/2019).

Author Contributions

A Chakravarthy: conceptualization, validation, investigation, visualization, methodology, and writing—original draft, review, and editing.
A Nandakumar: conceptualization, data curation, software, formal analysis, visualization, and writing—original draft, review, and editing.
G George: conceptualization, validation, investigation, visualization, methodology, and writing—original draft, review, and editing.
S Ranganathan: resources, data curation, software, and formal analysis.
S Umashankar: validation, investigation, and methodology.
N Shettigar: validation, investigation, and methodology.
D Palakodeti: resources and data curation.
A Gulyani: conceptualization, supervision, funding acquisition, visualization, and writing—original draft, review, and editing.
A Ramesh: conceptualization, supervision, funding acquisition, visualization, and writing—original draft, review, and editing.

Conflict of Interest Statement

A Ramesh, A Gulyani., A Chakravarthy, and G George are inventors on a patent application related to this study (Indian Complete Patent Application No. 202041030231). The authors declare no other competing interests.

References

1. Wu F, Zhao S, Yu B, Chen Y-M, Wang W, Song Z-G, Hu Y, Tao Z-W, Tian J-H, Pei Y-Y, et al (2020) A new coronavirus associated with human respiratory disease in China. *Nature* 579: 265–269. doi:10.1038/s41586-020-2008-3
2. Clinical spectrum | COVID-19 treatment guidelines. https://www.covid19treatmentguidelines.nih.gov/overview/clinical-spectrum/.
3. Wiersinga WJ, Rhodes A, Cheng AC, Peacock SJ, Prescott HC (2020) Pathophysiology, transmission, diagnosis, and treatment of coronavirus disease 2019 (COVID-19): A review. *JAMA* 324: 782–793. doi:10.1001/jama.2020.12839
4. Pfefferle S, Reucher S, Nörz D, Lütgehetmann M (2020) Evaluation of a quantitative RT-PCR assay for the detection of the emerging coronavirus SARS-CoV-2 using a high throughput system. *Euro Surveill* 25: 2000152. doi:10.2807/1560-7917.ES.2020.25.9.2000152
5. Mak GC, Cheng PK, Lau SS, Wong KK, Lau CS, Lam ET, Chan RC, Tsang DN (2020) Evaluation of rapid antigen test for detection of SARS-CoV-2 virus. *J Clin Virol* 129: 104500. doi:10.1016/j.jcv.2020.104500
6. Schnurra C, Reiners N, Biemann R, Kaiser T, Trawinski H, Jassoy C (2020) Comparison of the diagnostic sensitivity of SARS-CoV-2 nucleoprotein and glycoprotein-based antibody tests. *J Clin Virol* 129: 104544. doi:10.1016/j.jcv.2020.104544
7. Vogels CBF, Brito AF, Wyllie AL, Fauver JR, Ott IM, Kalinich CC, Petrone ME, Casanovas-Massana A, Catherine Muenker M, Moore AJ, et al (2020) Analytical sensitivity and efficiency comparisons of SARS-CoV-2 RT-qPCR primer-probe sets. *Nat Microbiol* 5: 1299–1305. doi:10.1038/s41564-020-0761-6
8. Antigen-detection in the diagnosis of SARS-CoV-2 infection using rapid immunoassays. https://www.who.int/publications/i/item/antigen-detection-in-the-diagnosis-of-sars-cov-2infection-using-rapid-immunoassays.
9. Corman VM, Landt O, Kaiser M, Molenkamp R, Meijer A, Chu DK, Bleicker T, Brünink S, Schneider J, Schmidt ML, et al (2020) Detection of 2019 novel coronavirus (2019-nCoV) by real-time RT-PCR. *Euro Surveill* 25: 2000045. doi:10.2807/1560-7917.ES.2020.25.3.2000045
10. Pearson JD, Trcka D, Lu S, Hyduk SJ, Jen M, Aynaud MM, Hernández JJ, Peidis P, Barrios-Rodiles M, Chan K, et al (2021) Comparison of SARS-CoV-2 indirect and direct RT-qPCR detection methods. *Virol J* 18: 99. doi:10.1186/s12985-021-01574-4
11. Emergency Use Authorization | FDA. https://www.fda.gov/emergency-preparedness-and-response/mcm-legal-regulatory-and-policy-framework/emergency-use-authorization.
12. Icmr (2003) Performance evaluation of commercial kits for real time PCR for covid by ICMR identified validation centres. https://www.icmr.gov.in/pdf/covid/kits/RT_PCR_Tests_Kits_Evaluation_Summ_20072021.pdf.
13. SARS-CoV-2 diagnostic pipeline: find. https://www.finddx.org/covid-19/pipeline/?avance=all&type=all&test_target=RNA&status=all&section=show-all&action=default.
14. Thi VLD, Herbst K, Boerner K, Meurer M, Kremer LP, Kirrmaier D, Freistaedter A, Papagiannidis D, Galmozzi C, Stanifer ML, et al (2020) A colorimetric RT-LAMP assay and LAMP-sequencing for detecting SARS-CoV-2 RNA in clinical samples. *Sci Transl Med* 12: eabc7075. doi:10.1126/scitranslmed.abc7075. http://stm.sciencemag.org/
15. Yan C, Cui J, Huang L, Du B, Chen L, Xue G, Li S, Zhang W, Zhao L, Sun Y, et al (2020) Rapid and visual detection of 2019 novel coronavirus (SARS-CoV-2) by a reverse transcription loop-mediated isothermal amplification assay. *Clin Microbiol Infect* 26: 773–779. doi:10.1016/j.cmi.2020.04.001
16. Kellner MJ, Ross JJ, Schnabl J, Dekens MPS, Heinen R, Tanner NA, Fritsche-Polanz R, Traugott M, Seitz T, Zoufaly A, et al (2020) Scalable, rapid and highly sensitive isothermal detection of SARS-CoV-2 for laboratory and home testing. *BioRxiv*. doi:10.1101/2020.06.23.166397 (Preprint posted June 23, 2020).
17. Gadkar VJ, Goldfarb DM, Gantt S, Tilley PAG (2018) Real-time detection and monitoring of loop mediated amplification (LAMP) reaction using self-quenching and de-quenching fluorogenic probes. *Sci Rep* 8: 5548–5610. doi:10.1038/s41598-018-23930-1

18. Sahoo PR, Sethy K, Mohapatra S, Panda D (2016) Loop mediated isothermal amplification: An innovative gene amplification technique for animal diseases. *Vet World* 9: 465–469. doi:10.14202/vetworld.2016.465-469

19. Joung J, Ladha A, Saito M, Kim NG, Woolley AE, Segel M, Barretto RPJ, Ranu A, Macrae RK, Faure G, et al (2020) Detection of SARS-CoV-2 with SHERLOCK one-pot testing. *N Engl J Med* 383: 1492–1494. doi:10.1056/nejmc2026172

20. Patchsung M, Jantarug K, Pattama A, Aphicho K, Suraritdechachai S, Meesawat P, Sappakhaw K, Leelahakorn N, Ruenkam T, Wongsatit T, et al (2020) Clinical validation of a Cas13-based assay for the detection of SARS-CoV-2 RNA. *Nat Biomed Eng* 4: 1140–1149. doi:10.1038/s41551-020-00603-x

21. Arizti-Sanz J, Freije CA, Stanton AC, Petros BA, Boehm CK, Siddiqui S, Shaw BM, Adams G, Kosoko-Thoroddsen TF, Kemball ME, et al (2020) Streamlined inactivation, amplification, and Cas13-based detection of SARS-CoV-2. *Nat Commun* 11: 5921. doi:10.1038/s41467-020-19097-x

22. Broughton JP, Deng X, Yu G, Fasching CL, Servellita V, Singh J, Miao X, Streithorst JA, Granados A, Sotomayor-Gonzalez A, et al (2020) CRISPR-Cas12-based detection of SARS-CoV-2. *Nat Biotechnol* 38: 870–874. doi:10.1038/s41587-020-0513-4

23. Azhar M, Phutela R, Kumar M, Ansari AH, Rauthan R, Gulati S, Sharma N, Sinha D, Sharma S, Singh S, et al (2020). Rapid, accurate, nucleobase detection using FnCas9. *MedRxiv*. doi:10.1101/2020.09.13.20193581. (Preprint posted September 14, 2020).

24. Fozouni P, Son S, Díaz de León Derby M, Knott GJ, Gray CN, D'Ambrosio MV, Zhao C, Switz NA, Kumar GR, Stephens SI, et al (2020) Amplification-free detection of SARS-CoV-2 with CRISPR-Cas13a and mobile phone microscopy. *Cell* 184: 1–11. doi:10.1016/j.cell.2020.12.001

25. Jung JK, Alam KK, Verosloff MS, Capdevila DA, Desmau M, Clauer PR, Lee JW, Nguyen PQ, Pastén PA, Matiasek SJ, et al (2020) Cell-free biosensors for rapid detection of water contaminants. *Nat Biotechnol* 38: 1451–1459. doi:10.1038/s41587-020-0571-7

26. Trachman RJ, Ferré-D'Amaré AR (2019) Tracking RNA with light: Selection, structure, and design of fluorescence turn-on RNA aptamers. *Q Rev Biophys* 52: e8. doi:10.1017/S0033583519000064

27. Pardee K, Green AA, Takahashi MK, Braff D, Lambert G, Lee JW, Ferrante T, Ma D, Donghia N, Fan M, et al (2016) Rapid, low-cost detection of zika virus using programmable biomolecular components. *Cell* 165: 1255–1266. doi:10.1016/j.cell.2016.04.059

28. Ma D, Shen L, Wu K, Diehnelt CW, Green AA (2018) Low-cost detection of norovirus using paper-based cell-free systems and synbody-based viral enrichment. *Synth Biol (Oxf)* 3: ysy018. doi:10.1093/synbio/ysy018

29. Takahashi MK, Tan X, Dy AJ, Braff D, Akana RT, Furuta Y, Donghia N, Ananthakrishnan A, Collins JJ (2018) A low-cost paper-based synthetic biology platform for analyzing gut microbiota and host biomarkers. *Nat Commun* 9: 3347–3412. doi:10.1038/s41467-018-05864-4

30. Wang S, Emery NJ, Liu AP (2019) A novel synthetic toehold switch for MicroRNA detection in mammalian cells. *ACS Synth Biol* 8: 1079–1088. doi:10.1021/acssynbio.8b00530

31. Green AA, Silver PA, Collins JJ, Yin P (2014) Toehold switches: De-novo-designed regulators of gene expression. *Cell* 159: 925–939. doi:10.1016/j.cell.2014.10.002

32. Pardee K, Green AA, Ferrante T, Cameron DE, DaleyKeyser A, Yin P, Collins JJ (2014) Paper-based synthetic gene networks. *Cell* 159: 940–954. doi:10.1016/j.cell.2014.10.004

33. Hao Y, Li J, Li Q, Zhang L, Shi J, Zhang X, Aldalbahi A, Wang L, Fan C, Wang F (2020) Programmable live-cell CRISPR imaging with toehold-switch-mediated strand displacement. *Angew Chem Int Ed Engl* 59: 20612–20618. doi:10.1002/anie.202009062

34. Hong F, Ma D, Wu K, Mina LA, Luiten RC, Liu Y, Yan H, Green AA (2020) Precise and programmable detection of mutations using ultraspecific riboregulators. *Cell* 180: 1018–1032.e16. doi:10.1016/j.cell.2020.02.011

35. Compton J (1991) Nucleic acid sequence-based amplification. *Nature* 350: 91–92. doi:10.1038/350091a0

36. Revets H, Marissens D, De Wit S, Lacor P, Clumeck N, Lauwers S, Zissis G (1996) Comparative evaluation of NASBA HIV-1 RNA QT, AMPLICOR-HIV monitor, and QUANTIPLEX HIV RNA assay, three methods for quantification of human immunodeficiency virus type 1 RNA in plasma. *J Clin Microbiol* 34: 1058–1064. doi:10.1128/jcm.34.5.1058-1064.1996

37. Loeffler J, Hebart H, Cox P, Flues N, Schumacher U, Einsele H (2001) Nucleic acid sequence-based amplification of Aspergillus RNA in blood samples. *J Clin Microbiol* 39: 1626–1629. doi:10.1128/JCM.39.4.1626-1629.2001

38. Uyttendaele M, Schukkink R, Van Gemen B, Debevere J (1995) Detection of Campylobacter jejuni added to foods by using a combined selective enrichment and nucleic acid sequence-based amplification (NASBA). *Appl Environ Microbiol* 61: 1341–1347. doi:10.1128/aem.61.4.1341-1347.1995

39. Romano JW, Van Gemen B, Kievits T (1996) NASBA: A novel, isothermal detection technology for qualitative and quantitative HIV-1 RNA measurements. *Clin Lab Med* 16: 89–103. doi:10.1016/s0272-2712(18)30289-0

40. Gracias KS, McKillip JL (2007) Nucleic acid sequence-based amplification (NASBA) in molecular bacteriology: A procedural guide. *J Rapid Methods Auto Microbiol* 15: 295–309. doi:10.1111/j.1745-4581.2007.00099.x

41. Guatelli JC, Whitfield KM, Kwoh DY, Barringer KJ, Richman DD, Gingeras TR (1990) Isothermal, in vitro amplification of nucleic acids by a multienzyme reaction modeled after retroviral replication. *Proc Natl Acad Sci U S A* 87: 1874–1878. doi:10.1073/pnas.87.5.1874

42. van Deursen PBH, Gunther AW, Spaargaren-van Riel CC, van den Eijnden MMED, Vos HL, van Gemen B, van Strijp DAMW, Tacken NMM, Bertina RM (1999) A novel quantitative multiplex NASBA method: Application to measuring tissue factor and CD14 mRNA levels in human monocytes. *Nucleic Acids Res* 27: e15. doi:10.1093/nar/27.17.e15-i

43. Abdolahzadeh A, Dolgosheina EV, Unrau PJ (2019) RNA detection with high specificity and sensitivity using nested fluorogenic Mango NASBA. *RNA* 25: 1806–1813. doi:10.1261/rna.072629.119

44. Cherian S, Yadav P, Potdar V, Choudhary M, Nyayanit D, Agrawal M, Jadhav S, Majumdar T, Shete-Aich A, Basu A, et al (2020) Full-genome sequences of the first two SARS-CoV-2 viruses from India. *Indian J Med Res* 151: 200–209. doi:10.4103/ijmr.IJMR_663_20

45. Untergasser A, Cutcutache I, Koressaar T, Ye J, Faircloth BC, Remm M, Rozen SG (2012) Primer3: New capabilities and interfaces. *Nucleic Acids Res* 40: e115. doi:10.1093/nar/gks596

46. Zadeh JN, Steenberg CD, Bois JS, Wolfe BR, Pierce MB, Khan AR, Dirks RM, Pierce NA (2011) Nupack: Analysis and design of nucleic acid systems. *J Comput Chem* 32: 170–173. doi:10.1002/jcc.21596

47. Pelisek J, Armeanu S, Nikol S (2000) Evaluation of β-galactosidase activity in tissue in the presence of blood. *J Vasc Res* 37: 585–593. doi:10.1159/000054092

48. Walsh KA, Jordan K, Clyne B, Rohde D, Drummond L, Byrne P, Ahern S, Carty PG, O'Brien KK, O'Murchu E, et al (2020) SARS-CoV-2 detection, viral load and infectivity over the course of an infection. *J Infect* 81: 357–371. doi:10.1016/j.jinf.2020.06.067

49. Hasanoglu I, Korukluoglu G, Asilturk D, Cosgun Y, Kalem AK, Altas AB, Kayaaslan B, Eser F, Kuzucu EA, Guner R (2020) Higher viral loads in asymptomatic COVID-19 patients might be the invisible part of the iceberg. *Infection* 1: 3. doi:10.1007/s15010-020-01548-8

50. Wyllie AL, Fournier J, Casanovas-Massana A, Campbell M, Tokuyama M, Vijayakumar P, Warren JL, Geng B, Muenker MC, Moore AJ, et al (2020) Saliva or nasopharyngeal swab specimens for detection of SARS-CoV-2. *N Engl J Med* 383: 1283–1286. doi:10.1056/nejmc2016359

51. Pujadas E, Chaudhry F, McBride R, Richter F, Zhao S, Wajnberg A, Nadkarni G, Glicksberg BS, Houldsworth J, Cordon-Cardo C (2020) SARS-CoV-2 viral load predicts COVID-19 mortality. *Lancet Respir Med* 8: e70. doi:10.1016/S2213-2600(20)30354-4

52. Wu Q, Suo C, Brown T, Wang T, Teichmann SA, Bassett AR (2021) INSIGHT: A population-scale COVID-19 testing strategy combining point-of-care diagnosis with centralized high-throughput sequencing. *Sci Adv* 7: 5054–5066. doi:10.1126/sciadv.abe5054

53. Rabe BA, Cepko C (2020) SARS-CoV-2 detection using isothermal amplification and a rapid, inexpensive protocol for sample inactivation and purification. *Proc Natl Acad Sci U S A* 117: 24450–24458. doi:10.1073/pnas.2011221117

54. Wu Q, Suo C, Brown T, Wang T, Teichmann S, Bassett A (2020) INSIGHT: A population scale COVID-19 testing strategy combining point-of-care diagnosis with centralised high-throughput sequencing. *BioRxiv*. doi:10.1101/2020.06.01.127019. (Preprint posted August 16, 2020).

55. Vogels CBF, Watkins AE, Harden CA, Brackney DE, Shafer J, Wang J, Caraballo C, Kalinich CC, Ott IM, Fauver JR, et al (2021) SalivaDirect: A simplified and flexible platform to enhance SARS-CoV-2 testing capacity. *Med (N Y)* 2: 263–280.e6. doi:10.1016/j.medj.2020.12.010

56. Torjesen I (2021) Covid-19: Delta variant is now UK's most dominant strain and spreading through schools. *BMJ* 373: n1445. doi:10.1136/bmj.n1445

57. Callaway E (June 2021) Delta coronavirus variant: Scientists brace for impact. *Nature* 595: 17–18. doi:10.1038/d41586-021-01696-3

58. O'Dowd A (2021) Covid-19: Cases of delta variant rise by 79%, but rate of growth slows. *BMJ* 373: n1596. doi:10.1136/bmj.n1596

59. Morabito K, Wiske C, Tripathi A (2013) Engineering insights for multiplexed real-time nucleic acid sequence-based amplification (NASBA): Implications for design of point-of-care diagnostics. *Mol Diagn Ther* 17: 185–192. doi:10.1007/s40291-013-0029-4

60. Schindelin J, Arganda-Carreras I, Frise E, Kaynig V, Longair M, Pietzsch T, Preibisch S, Rueden C, Saalfeld S, Schmid B, et al (2012) Fiji: An open-source platform for biological-image analysis. *Nat Methods* 9: 676–682. doi:10.1038/nmeth.2019

61. Deiman B, Van Aarle P, Sillekens P (2002) Characteristics and applications of nucleic acid sequence-based amplification (NASBA). *Mol Biotechnol* 20: 163–179. doi:10.1385/MB:20:2:163